Wollastonite-containing bioceramic coatings on alumina substrates: design considerations and mechanical modelling

Francesco Baino*, Chiara Vitale-Brovarone

[a] *Institute of Materials Physics and Engineering, Applied Science and Technology Department, Politecnico di Torino, Corso Duca degli Abruzzi 24, 10129 Torino, Italy*

* Corresponding author: F. Baino

Tel.: +39 011 090 4668

Fax: +39 011 090 4624

E-mail: francesco.baino@polito.it

Abstract

In this work we produced wollastonite-containing glass-ceramic coatings on alumina substrates by airbrush spraying of glass-based aqueous suspensions followed by sintering. Investigations by scanning electron microscopy revealed that layer-wise slurry deposition is a suitable technique to manufacture homogeneous and continuous bioceramic coatings without flaws or cracks at the coating/substrate interface. Coating thickness can be designed by controlling the number of spraying cycles. The bonding strength of the coating (about 22 MPa) was found adequate for biomedical applications. A mechanical model based on the innovative concepts of quantized fracture mechanics was developed to predict the bonding strength and estimate the fracture toughness of the coating on the basis of experimental data from tensile tests. The approach proposed in this work can contribute to optimize the design and manufacturing of bioceramic coatings with the aim of improving their mechanical properties and suitability for clinical applications.

Keywords: Bioceramics; Coating; Fracture mechanics; Modelling.

1. Introduction

Bioceramics have been investigated and used for decades for a number of biomedical applications, including small bone substitutions, implantable drug delivery systems, bone cements and non-load-bearing implants [1,2]. However, their use has been limited by their poor mechanical properties and intrinsic brittleness. In order to overcome these shortcomings, bioceramics have been successfully proposed as coatings on tougher non-bioactive substrates, such as metal alloys or alumina, to promote a strong adhesion between implant and bone [3]. For instance, plasma-sprayed hydroxyapatite (HA) coatings have been employed in dentistry and orthopaedics for the last 30 years to improve implant fixation and bone tissue ingrowth at the bone/implant interface; unfortunately, many concerns still remain about the use of these coatings, mainly with regard to their long-term stability in the body environment [4].

Other methods have been reported in the literature to coat a substrate with a bioceramic layer, including enamelling [5], sol-gel dipping [6], spin coating [7], sputtering [8] and electrophoretic deposition [9,10]. In spite of these great research efforts much still has to be done to benefit fully from bioceramic coatings and, except for the case of thermally-sprayed HA, bioceramic coatings are rarely applied in the clinical practice. This opens new prospects for the scientific research in the hope that a truly functional coating – and a suitable method to produce it – will eventually materialize.

In this regard, bioactive glasses and glass-ceramics have attracted the researchers' interest as they have been demonstrated to form an interfacial bond with host bone tissue [11]. Very interestingly, it was assessed that the strength of the interfacial bond between bioactive glass and bone was equal to or greater than the strength of the host bone [12]. Therefore, this special set of bioceramics has

the potential to improve the stability of orthopaedic and dental implants by bonding them toughly to the host bone [13]. However, most bioactive glasses are by nature biodegradable with ultralow to fast dissolution kinetics (depending on the composition) [13], and therefore a highly bioactive coating made of them may degrade over time thereby causing instability of the prosthetic implant in the long term. Another crucial issue is associated to the different thermal behaviour of bioactive glasses/glass-ceramics and metallic/ceramic prosthetic substrate to be coated. When glass coatings are applied, the thermal expansion coefficient (TEC) of the glass should match that of the substrate to prevent the glass pulling away from the metal during processing [14]. This is a crucial issue for bioactive glasses since their TEC usually does not match that of biomedical metals (e.g. titanium) or inert bioceramics (e.g. alumina) [15]. An additional problem is that bioactive glasses usually crystallize upon sintering, and sintering is needed for a good coating. In order to match the TEC of the glass to that of titanium alloys, a number of variations of the original 45S5 Bioglass® composition ($45SiO_2$–$24.5CaO$–$24.5Na_2O$–$6P_2O_5$ wt.%) have been investigated, as comprehensively reviewed by Sola et al. in a valuable paper [16].

In the present work we addressed the fabrication and mechanical modelling of wollastonite-containing glass-ceramic coatings produced by airbrush spraying of a SiO_2–CaO–Na_2O–Al_2O_3 glass powder suspension on alumina substrates followed by thermal treatment. Airbrush spraying of ceramic slurries is a versatile strategy to produce coatings with good control of the thickness [17-20] and promising possibilities of scaling up from the "Lab scale" to industrial production. However, there is a relative paucity of studies concerning the layer-wise deposition of ceramic slurries for biomedical applications [21,22] and the full potentialities of this approach are still unexplored. We also developed a mechanical model based on the concepts of quantized fracture mechanics (QFM) [23] to describe the bonding strength of the glass-ceramic coating to the alumina substrate.

2. Materials and methods

2.1 Preparation of the samples

The flat ceramic substrates (10 mm × 10 mm square samples, thickness 1 mm) to be coated were obtained by cutting high-purity (> 99.5 wt.%) alumina sheets (Goodfellow, Cambridge, UK) by a diamond blade (Accutom 5 Machine, Struers). Before subsequent treatment the alumina substrates were washed with deionized water and acetone; the surface of the specimens was not abraded.

The material used for coating preparation was a silicate glass with the following molar composition: 57% SiO_2, 34% CaO, 6% Na_2O, 3% Al_2O_3 [24,25]. The glass reagents (high-purity powders of SiO_2, $CaCO_3$, Na_2CO_3 and Al_2O_3 purchased from Sigma-Aldrich) were molten in a platinum crucible at 1550 °C for 1 h in air; the melt was quenched in cold water to obtain a frit, that was subsequently ground by a 6-ball zirconia milling machine and sieved (stainless steel sieves, Giuliani Technologies Srl) to a final particle size below 32 μm. A glass-based slurry (weight formulation: 30% glass, 64% water, 6% poly(vinyl alcohol) (PVA) was prepared and then layer-wise deposited on the alumina substrates by an airbrush spray gun (Evolution Silverline M, Harder & Steenbeck, Germany). A schematic view of the process of slurry deposition by airbrush is reported in Fig. 1. Single green layers were dried at room temperature for 1 h at the end of each spraying cycle. Once all the depositions were completed, the samples were dried overnight under ambient conditions and subsequently thermally treated in an electrical furnace at 1000 °C for 3 h (heating and cooling rates were set at 5 and 10 °C min^{-1}, respectively).

2.2. Characterisation

Glass-derived coatings underwent wide-angle X-ray diffraction (XRD; 2θ within 10-70°) to assess the presence of crystalline phases. The analysis was performed by using a X'Pert Philips diffractometer operating at 40 kV and 30 mA with Bragg-Brentano camera geometry, Cu Kα

incident radiation (wavelength λ = 0.15405 nm), step size $\Delta(2\theta)$ = 0.02° and fixed counting time of 1 s per step. Crystalline phases were identified by using X'Pert HighScore program equipped with PCPDFWIN database.

The samples were embedded in epoxy resin (Epofix, Struers), cut and polished using #600 to #4000 SiC grit paper; the resulting cross-sections were metal-coated with silver and then analysed by scanning electron microscopy (SEM, Philips 525 M; working voltage: 15 kV).

Mechanical tests were performed according to the relevant ASTM standard [26] by applying tensile loads (Syntech 10/D machine, MTS Corp.; cross-head speed of 1 mm min^{-1}) to the samples up to failure. Before testing, each sample was glued to two loading fixtures (16-mm diameter steel cylinders) by using an epoxy resin (Araldite® AV 119, Ciba-Geigy), which is able to withstand stresses above 40 MPa (as declared by the manufacturer). The adhesive was a gel at room temperature; its polymerization was achieved by a low-temperature treatment in an oven (130 °C for 1 h). The failure tensile strength was calculated as L/A, where L (N) is the failure tensile load and A (mm^2) is the area on which the load was applied. The result was expressed as mean value ± standard deviation calculated on ten samples.

2.3. Mechanical modelling

According to the general principles of linear elastic fracture mechanics, the total potential energy Π of a system can be expressed as:

$$\Pi = U - W \tag{1}$$

wherein U is the strain energy and W is the work done by an external load L that acts on the system considered. In our case, the system of interest is represented by a flat square-shaped alumina substrate coated by a glass-derived sintered layer. U and W can be calculated as follows:

$$U = \frac{1}{2} L^2 \left(\frac{1}{k_c} + \frac{1}{k_s} \right) \tag{2}$$

$$W = L^2\left(\frac{1}{k_c}+\frac{1}{k_s}\right) \tag{3}$$

wherein k_c and k_s are the stiffness of coating and substrate, respectively, before crack propagation. Combining Eqs.(2) and (3), the total potential energy can be obtained as:

$$\Pi = -\frac{1}{2}L^2\left(\frac{1}{k_c}+\frac{1}{k_s}\right) \tag{4}$$

According to the concepts of QFM [23], a quantization of Griffith's criterion is assumed to account for discrete crack; thus in the continuum hypothesis, differentials are substituted with finite differences, i.e. $d \to \Delta$. Griffith's energy criterion implies a crack propagation when the variation of the total potential energy $d\Pi$, corresponding to a virtual increment of the crack surface dA, becomes equal to the energy spent to create the new free crack surface, i.e. $dW + G_{IC} \cdot dA = 0$, where G_{IC} is the fracture energy (per unit area created) of the material. In QFM, Griffith's equation can be rewritten as follows:

$$G_{IC} = -\frac{\Delta\Pi}{\Delta A} \tag{5}$$

In a first "ideal" scenario, we assume that failure occurs at the interface between coating and alumina substrate; therefore, the variation of the total potential energy can be calculated using Eq.(4) as:

$$\Delta\Pi = -\frac{1}{2}L^2\left[\left(\frac{1}{k_c^*}-\frac{1}{k_c}\right)+\left(\frac{1}{k_s^*}-\frac{1}{k_s}\right)\right] \tag{6}$$

wherein k_c^* and k_s^* are the stiffness of coating and substrate, respectively, after crack propagation. Having denoted as E_c and E_s the Young's moduli of coating and substrate, respectively, and having indicated t_c and t_s the corresponding thicknesses, we can express the compliances in Eq.(6) as:

$$\frac{1}{k_c^*}-\frac{1}{k_c} = \frac{t_c}{E_c A^2}\cdot\frac{\Delta A}{1-\frac{\Delta A}{A}} \tag{7}$$

$$\frac{1}{k_s^*}-\frac{1}{k_s}=\frac{t_s}{E_s A^2}\cdot\frac{\Delta A}{1-\frac{\Delta A}{A}} \tag{8}$$

Substituting Eqs.(7) and (8) into Eq.(6), we obtain:

$$\Delta\Pi=-\frac{1}{2}L^2\left(\frac{t_c}{E_c A^2}\cdot\frac{\Delta A}{1-\frac{\Delta A}{A}}+\frac{t_s}{E_s A^2}\cdot\frac{\Delta A}{1-\frac{\Delta A}{A}}\right) \tag{9}$$

Considering Eqs.(5) and (9), the energy release rate $G_{I,c\text{-}s}$ is finally obtained as:

$$G_{I,c-s}=-\frac{\Delta\Pi}{\Delta A}=\frac{1}{2}\left(\frac{L}{A}\right)^2\left(\frac{t_c}{E_c\left(1-\frac{\Delta A}{A}\right)}+\frac{t_s}{E_s\left(1-\frac{\Delta A}{A}\right)}\right)=\left(\sigma_{I,c-s}\right)^2\frac{E_s t_c+E_c t_s}{2E_c E_s\left(1-\frac{\Delta A}{A}\right)} \tag{10}$$

The crack propagation is unstable if $\frac{dG_{I,c-s}}{d(\Delta A)}>0$; calculation of the first-order derivative of Eq.(10) gives the following condition:

$$\frac{dG_{I,c-s}}{d(\Delta A)}=\left(\sigma_{I,c-s}\right)^2\frac{A(E_s t_c+E_c t_s)}{2E_c t_s(A-\Delta A)^2}>0 \tag{11}$$

from which we can conclude that crack propagation is always unstable.

Rearranging Eq.(10), the delamination strength can be finally expressed as:

$$\sigma_{IC,c-s}=\left(\frac{2E_c E_s}{E_s t_c+E_c t_s}G_{IC,c-s}\left(1-\frac{\Delta A}{A}\right)\right)^{0.5} \tag{12}$$

In a second "ideal" scenario, we assume that failure occurs in the coating, as its strength $\sigma_{IC,c}$ (i.e., the strength of the sintered glass-ceramic that constitutes the coating) is supposed to be lower than the bonding strength at the coating/substrate interface.

In a real case, such as the one reported in the present article, there is a coexistence between the two failure modes previously described. We assumed that the critical stress can be predicted by a mean field approach[1] as:

$$\sigma_{IC,m} = \sigma_{IC,c-s}\frac{A_d}{A} + \sigma_{IC,c}\left(1 - \frac{A_d}{A}\right) \tag{13}$$

wherein $A_d = A - \Delta A$ is the final delamination area and the subscript "m" denotes the mixed cracking mode. Therefore, Eq.(13) can be eventually rewritten as:

$$\sigma_{IC,m} = \left(\frac{2E_cE_s}{E_st_c + E_ct_s}G_{IC,c-s}\frac{A_d}{A}\right)^{0.5}\frac{A_d}{A} + \sigma_{IC,c}\left(1 - \frac{A_d}{A}\right) \tag{14}$$

3. Results and discussion

One crystalline phase, identified as wollastonite ($CaSiO_3$, code no. 00-027-0088), was detected in the thermally-treated coating (Fig. 2); this phase is known to be highly biocompatible and suitable for applications in the biomedical field [27]. This finding is consistent with previous results by the authors, who reported the development of this phase after thermal treatment of SiO_2-CaO-Na_2O-Al_2O_3 glasses above 900 °C [28,29]. It was also demonstrated elsewhere that this type of glass-ceramic material exhibits a moderate ability to induce formation of surface apatite *in vitro* together with an excellent durability in a biological environment [24], which are very interesting features for bioceramic coatings intended to interact with bone tissue and ensure a long-term stability of the implant.

Airbrush spraying of SiO_2-CaO-Na_2O-Al_2O_3 glass suspensions demonstrated to be an effective method to produce continuous coatings with homogeneous thickness along the cross-section, without cracks or delamination at the interface with the alumina substrate (Figs. 3a and b). The top-view of a typical coating shown in Fig. 3c reveals that an excellent densification of the glass

[1] The mean field approach allows a given parameter x_m to be expressed as $x_m = \sum_i^n \xi_i x_i$, where x_i are the (known) constituents and $\sum_i^n \xi_i = 1$.

particles deposited via airbrushing was achieved upon heat treatment. Comparing these results with those available in the literature, it is instructive to observe that, for instance, the calcium phosphate and zirconia coatings produced via airbrushing by Pardun et al. [22] displayed a rougher, more irregular and inhomogeneous morphology. On the other hand, it is also interesting to underline that a recurrent problem of glass/glass-ceramic coatings on biomedical implants is the post-sintering cracking, which was not observed in the present work. This issue, however, is primarily due to the mismatch between the TEC of glass and substrate with associated interfacial stresses rather than to the method of coating deposition [30]. Good thermal matching between alumina (TEC = 8.5×10^{-6} $°C^{-1}$) and SiO_2-CaO-Na_2O-Al_2O_3 glass used in this work (TEC = 8.7×10^{-6} $°C^{-1}$ [24]) allowed high-quality sintered coatings to be obtained.

An increase of the coating thickness seemed to be associated to a higher number of defects (pores) in the coating (Fig. 3b). Specifically, the presence of longitudinal, elongated pores roughly parallel to the interface can be related to air entrapment between adjacent layers deposited with subsequent spraying cycles. Furthermore, PVA burn-off during the thermal treatment is accompanied by development of gases and, therefore, can contribute to the formation of these cavities.

The quality of adhesion between coating and alumina substrate after thermal treatment was very good; as already mentioned above, this was due to the good matching between the TECs of alumina and glass. In this regard, Fig. 4a qualitatively shows an excellent adhesion between substrate and coating, without interfacial cracks or flaws. The glass-ceramic nature of the coating is also visible in Fig. 4a, where Si-/Ca-rich "white" areas characterized by a needle-like morphology typical of wollastonite crystals (Fig. 4b) are embedded in a dark glassy matrix (Fig. 4c).

It is interesting to report a few considerations about the relationship between coating thickness (t) and number of airbrush spraying cycles (N), which could be crucial for scaling-up the process from "Lab research level" to industrial application. SEM investigations revealed that, from a general viewpoint, the value of t increases with the increment of N. In this study some important processing variables such as air pressure, nozzle diameter, velocity of the spraying movement and distance

from nozzle to substrate (Fig. 1) were kept constant. Hence we can assume that, having maintained constant the above mentioned parameters, the coating thickness is only dependent on the number of spraying cycles. Therefore, the coating thickness t can be related to N by means of a mathematical function with the initial condition t(N = 0) = 0. Two types of polynomial functions, linear and quadratic, were used for the interpolation. The model constants *a* and *b*, referring to the general expression $t = aN^2 + bN$, as well as the coefficients of determination R^2 are reported in Table 1. Comparison among the fitting curves and the experimental data is reported in Fig. 5. Fitting results exhibit good agreements with experimental data, as demonstrated by the high values of the coefficients R^2, which also reveals the good predictive capability of the presented approaches. Fitting by a quadratic function is preferable compared to linear interpolation as revealed by the higher value of R^2. The obtained interpolating functions can be a valuable tool at the designer's disposal to link the thickness of final coating with one of the key processing parameters – the number of spraying cycles, N – that can be easily controlled during the coating fabrication. In this regard, the analytical model describing the t-N relationship can be successfully employed for a "predictive purpose" and not only in a "descriptive way": in fact, knowing the coating thickness recommended or, in general, suitable for a given application, it is possible to purposely control the number of spraying cycles so that the coating can fulfil the desired requirement. This strategy would allow overcoming the limitations of conventional "trial-and-error" approach (loss of experimental time for preparation and subsequent checking of samples) and could be easily implemented on production lines for the industrial manufacturing of bioceramic coatings.

As suggested by the micrograph displayed in Fig. 3b, an increase in the coating thickness seems to yield a higher number of defects in the coating, which are known to be unavoidably associated to a decrement of the strength [31]. Therefore, only the coatings with thickness below 200 μm and, accordingly, very few rounded (closed) pores, such as the coating shown in Fig. 3a, can be considered actually promising for biomedical applications.

The failure strength of the coatings produced by applying 6 airbrush spraying cycles (Fig. 3a) was 22.3 ± 5.1 MPa; this result is comparable to that obtained in the case of analogous coatings produced on curved alumina substrates by the same method [21]. Glass-ceramic coatings produced by conventional enamelling on flat alumina substrates yielded similar values of failure strength, albeit slightly lower (around 20 MPa) [24]. The international standard ISO 13779 prescribes a tensile stress of at least 15 MPa for HA coatings on surgical implants [32]; therefore, the strength of the airbrush sprayed coatings produced in this work suggests their mechanical suitability for biomedical use.

The critical strain energy release rate was calculated by applying Eq.(14) and using the following parameters as model inputs: E_c = 90 GPa, E_s = 400 GPa, $\sigma_{IC,c}$ = 47 MPa (from previous works [28,33]), A = 100 mm^2, t_c = 140 μm, t_s = 1 mm (from the system geometry). Fitting of the experimental data ($\sigma_{IC,m}$ and A_d, assessed for each sample after the mechanical test) to estimate the unknown parameter of the model was carried out by using a software code based on the least mean square (LMS) algorithm. The best fitting of the experimental data gives $G_{IC,c-s}$ = 8.0×10^{-1} J m^{-2}, which can be interpreted as an estimation of fracture toughness [23]. Good agreement with experimental data (Fig. 6) is demonstrated by the high value of the coefficient of determination (R^2 = 0.805). Estimation of fracture toughness is a complex issue and there is a relative paucity of reports that deal with bioceramic coating. The value of $G_{IC,c-s}$ assessed in this work is almost twice as high as that reported in the case of glass-ceramic coatings produced by conventional enamelling on flat alumina substrates (4.6×10^{-1} J m^{-2}) [28].

4. Conclusions

Wollastonite-containing glass-ceramic coatings were prepared by airbrush spraying of glass-based slurry followed by high-temperature thermal treatment. This technique of deposition proved to be

suitable to obtain continuous, well adherent coatings with homogeneous thickness that can be modulated depending on the number of spraying cycles. The bonding strength of the coating to the alumina substrate (around 22 MPa) overpasses the minimum threshold value recommended by ISO standard for bioceramic coatings, which suggests the material suitability for biomedical use. The bonding strength of the coating was also investigated following an approach based on the combination between experimental results and QFM theory. By fitting the experimental data with the theoretical prediction, the fracture toughness of the system was estimated. The model and concepts reported in this article represent a novel approach towards a more rational design of bioceramic coatings for bone tissue engineering applications.

Acknowledgments

This work was supported by the EU-funded project MATCh ("Monoblock acetabular cup with trabecular-like coating", Grant no. 286548).

References

[1] L.L. Hench, Bioceramics, J. Am. Ceram. Soc. 81 (1998) 1705-1728.

[2] M. Vallet-Regi, E. Ruiz-Hernandez, Bioceramics: from bone regeneration to cancer nanomedicine, Adv. Mater. 23 (2011) 5177-5218.

[3] Y. Ramaswamy, C. Wu, H. Zreiqat, Orthopaedic coating materials: considerations and applications, Exp. Rev. Med. Devices 6 (2009) 423-430.

[4] L. Sun, C.C. Berndt, K.A. Gross, A. Kucuk, Material fundamentals and clinical performance of plasma-sprayed hydroxyapatite coatings: a review, J. Biomed. Mater. Res. (Appl. Biomater.) 58 (2001) 570-592.

[5] C. Vitale-Brovarone, E. Verné, SiO_2-CaO-K_2O coatings on alumina and Ti6Al4V substrates for biomedical applications, J. Mater. Sci. Mater. Med. 16 (2005) 863-871.

[6] M.H. Fathi, A. Doostmohammadi, Bioactive glass nanopowder and bioglass coating for biocompatibility improvement of metallic implant, J. Mater. Proc. Technol. 209 (2009) 1385-1391.

[7] X. Wang, X. Li, K. Onuma, A. Ito, Y. Sogo, K. Kosuge, A. Oyane, Mesoporous bioactive glass coatings on stainless steel for enhanced cell activity, cytoskeletal organization and AsMg immobilization, J. Mater. Chem. 20 (2010) 6437-6445.

[8] Y. Yang, K.H. Kim, J.L. Ong, A review on calcium phosphate coatings produced using a sputtering process – an alternative to plasma spraying, Biomaterials 26 (2005) 327-337.

[9] A.R. Boccaccini, S. Keim, R. Ma, Y. Li, I. Zhitomirsky, Electrophoretic deposition of biomaterials, J. R. Soc. Interface 7 (2010) S581-S613.

[10] S. Fiorilli, F. Baino, V. Cauda, M. Crepaldi, C. Vitale-Brovarone, D. Demarchi, B. Onida, Electrophoretic deposition of mesoporous bioactive glass on glass-ceramic foam scaffolds for bone tissue engineering, J. Mater. Sci. Mater. Med. 26 (2015) 21.

[11] L.L. Hench, R.J. Splinter, W.C. Allen, T.K. Greenlee , Bonding mechanisms at the interface of ceramic prosthetic materials, J. Biomed. Mater. Res. 5 (1972) 117-141.

[12] A.M. Weinstein, J.J. Klawitter, S.D. Cook, Implant-bone interface characteristics of Bioglass dental implants, J. Biomed. Mater. Res. 14 (1980) 23-29.

[13] J.R. Jones, Review of bioactive glass: from Hench to hybrids, Acta Biomater. 9 (2013) 4457-4486.

[14] J.M. Gomez-Vega, E. Saiz, A.P. Tomsia, T. Oku, K. Suganuma, G.W. Marshall, S.J. Marshall, Novel bioactive functionally graded coatings on Ti6Al4V, Adv. Mater. 12 (2000) 894-898.

[15] D. Bellucci, V. Cannillo, A. Sola, Coefficient of thermal expansion of bioactive glasses: available literature data and analytical equation estimates, Ceram. Int. 37 (2011) 2963-2972.

[16] A. Sola, D. Bellucci, V. Cannillo, A. Cattini, Bioactive glass coatings: a review, Surf. Eng. 27 (2011) 560-572.

[17] A. Ruder, H.P. Buchkremer, H. Jansen, W. Mallener, D. Stoever, Wet powder spraying - a process for the production of coatings, Surf. Coatings Technol. 53 (1992) 71-74.

[18] C.E.P. Willoughby, J.R.G. Evans, The preparation of laminated ceramic composites using paint technology, J. Mater. Sci. 31 (1996) 2333-2337.

[19] R. Polanco, P. Miranzo, M.I. Osendi, Fabrication and microstructure of a ZrO_2-Ni functionally graded bonding interlayer using the airbrush spraying method, Acta Mater. 54 (2006) 2215-2222.

[20] A.M. Waetjen, D.A. Polsakiewicz, I. Kuhl, R. Telle, H. Fischer, Slurry deposition by airbrush for selective laser sintering of ceramic components, J. Eur. Ceram. Soc. 29 (2009) 1-6.

[21] F. Baino, C. Vitale-Brovarone, Feasibility of glass-ceramic coatings on alumina prosthetic implants by airbrush spraying method, Ceram. Int. 41 (2015) 2150-2159.

[22] K. Pardun, L. Treccani, E. Volkmann, G. Li Destri, G. Marletta, P. Strecbein, C. Heiss, K. Rezwan, Characterization of wet powder-sprayed zirconia/calcium phosphate coating for dental implants, Clin. Implant. Dent. Relat. Res. 17 (2015) 186-198.

[23] N. Pugno, R. Ruoff, Quantized fracture mechanics, Philos. Mag. 84 (2004) 2829-2845.

[24] C. Vitale-Brovarone, F. Baino, F. Tallia, C. Gervasio, E. Verné, Bioactive glass-derived trabecular coating: a smart solution for enhancing osteointegration of prosthetic elements, J. Mater. Sci. Mater. Med. 23 (2012) 2369-2380.

[25] F. Baino, C. Vitale-Brovarone, Mechanical properties and reliability of glass-ceramic foam scaffolds for bone repair, Mater. Lett. 118 (2014) 27-30.

[26] ASTM C633 (2008). Standard test method for adhesion or cohesion strength of thermal spray coatings.

[27] T. Kokubo, S. Ito, S. Sakka, T. Yamamuro, Formation of a high-strength bioactive glass-ceramic in the system MgO-CaO-SiO_2-P_2O_5, J. Mater. Sci. 21 (1986) 536-540.

[28] Q. Chen, F. Baino, N.M. Pugno, C. Vitale-Brovarone, Bonding strength of glass-ceramic trabecular-like coatings to ceramic substrates for prosthetic applications, Mater. Sci. Eng. C 33 (2013) 1530-1538.

[29] H. Ma, F. Baino, S. Fiorilli, C. Vitale-Brovarone, B. Onida, Al-MCM-41 inside a glass-ceramic scaffold: a meso-macroporous system for acid catalysis, J. Eur. Ceram. Soc. 33 (2013) 1535-1543.

[30] D. Krause, B. Thomas, C. Leinenbach, D. Eifler, E.J. Minay, A.R. Boccaccini, The electrophoretic deposition of Bioglass® particles on stainless steel and Nitinol substrates, Surf. Coat. Technol. 200 (2006) 4835-4845.

[31] B.F. Sorensen, S. Primdahl, Relationship between strength and failure mode of ceramic multilayers, J. Mater. Sci. 33 (1998) 5291-5300.

[32] ISO 13779-4 (2002). Implants for surgery – Hydroxyapatite - Part 4: Determination of coating adhesion strength.

[33] Q. Chen, F. Baino, S. Spriano, N.M. Pugno, C. Vitale-Brovarone, Modelling of the strength-porosity relationship in glass-ceramic foam scaffolds for bone repair, J. Eur. Ceram. Soc. 34 (2014) 2663-2673.

Figure legends

Fig. 1. Experimental set-up used to manufacture the SiO_2-CaO-Na_2O-Al_2O_3 glass coatings by airbrush spraying: the slurry was deposited by a double-action airbrush from a distance of 100 mm and with an air pressure of 3.5×10^5 Pa; the airbrush nozzle diameter was 0.40 mm.

Fig. 2. XRD pattern of the thermally-treated glass-derived coating (1000 °C for 3 h).

Fig. 3. Morphological investigations of the coatings: cross-sectional SEM micrographs of sintered coatings (back-scattering mode) produced by applying (a) 6 airbrush spraying cycles and (b) 14 airbrush spraying cycles (both images were acquired with a magnification of 300×); (c) top view of a typical coating (SEM magnification: 200×). The coating thickness was measured by a specific tool of SEM software.

Fig. 4. Analysis of the coating: (a) SEM micrograph (2000×) showing the interface between coating (right) and alumina substrate (left) and EDS patterns of (b) the white areas (wollastonite crystals rich in Si and Ca) and (c) the dark areas (glassy phase; the EDS pattern shows high peaks for Na and Al) of the coating. The peak of silver (Ag) is due to the ultrathin metal coating needed for the analysis.

Fig. 5. Relationship between coating thickness (t) and number of spraying cycles (N); the dashed and solid lines correspond to, respectively, the linear and parabolic fitting of the experimental data. The model parameters are reported in Table 1.

Fig. 6. Mechanical modelling: comparison between model results and experimental data.

Tables

Table 1. Modelling of the relationship between coating thickness (t) and number of spraying cycles (N) through polynomial fitting (general function type: $t = aN^2 + bN$): model constants and coefficients of determination.

Model type	*a* (μm)	*b* (μm)	R^2
Linear	0	26.322	0.911
Parabolic	1.143	10.114	0.996

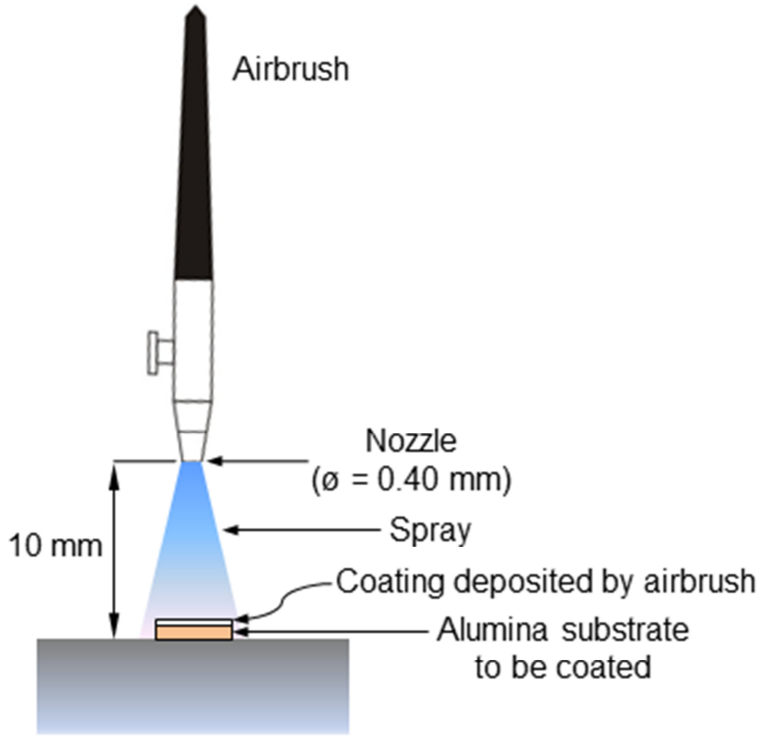
Airbrush
Nozzle
(ø = 0.40 mm)
10 mm
Spray
Coating deposited by airbrush
Alumina substrate
to be coated

Fig. 1

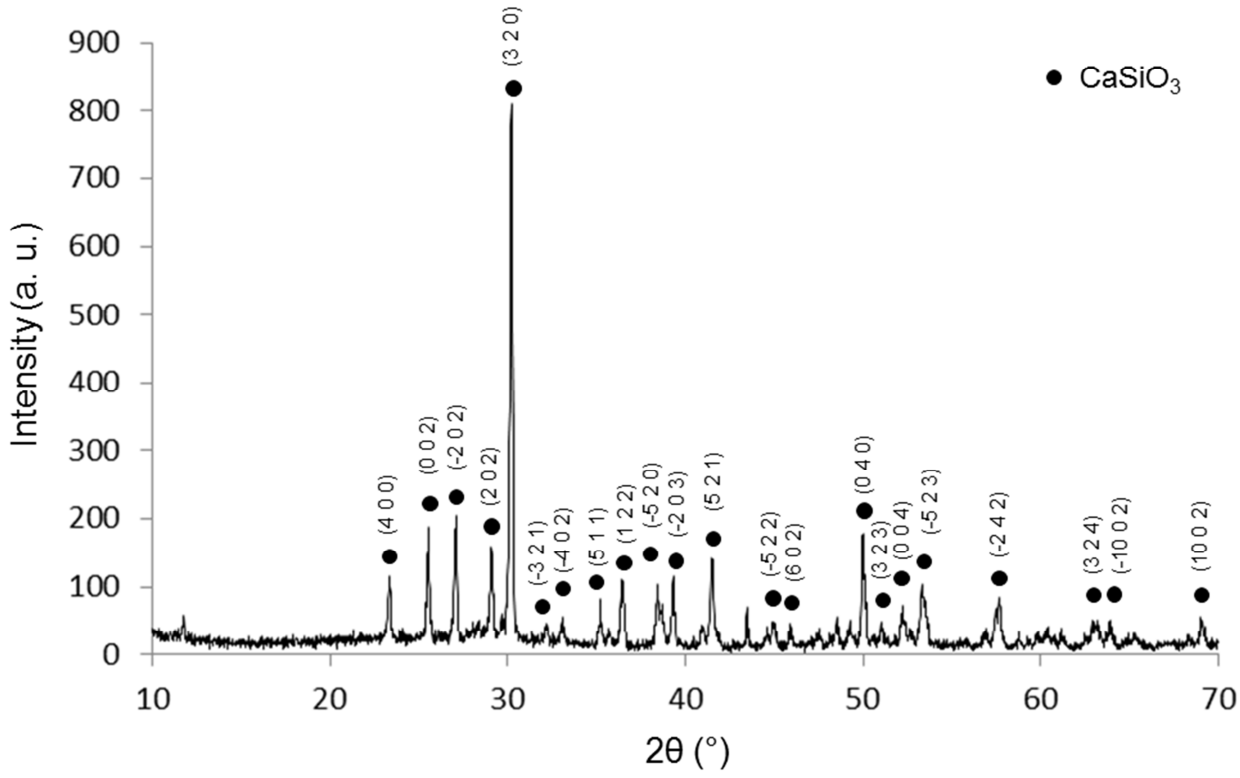
CaSiO3
Intensity (a. u.)
2θ (°)
0
100
200
300
400
500
600
700
800
900
10
20
30
40
50
60
70
(4 0 0)
(0 0 2)
(-2 0 2)
(2 0 2)
(3 2 0)
(-3 2 1)
(-4 0 2)
(5 1 1)
(1 2 2)
(-5 2 0)
(-2 0 3)
(5 2 1)
(-5 2 2)
(6 0 2)
(0 4 0)
(3 2 3)
(0 0 4)
(-5 2 3)
(-2 4 2)
(3 2 4)
(-10 0 2)
(10 0 2)

Fig. 2

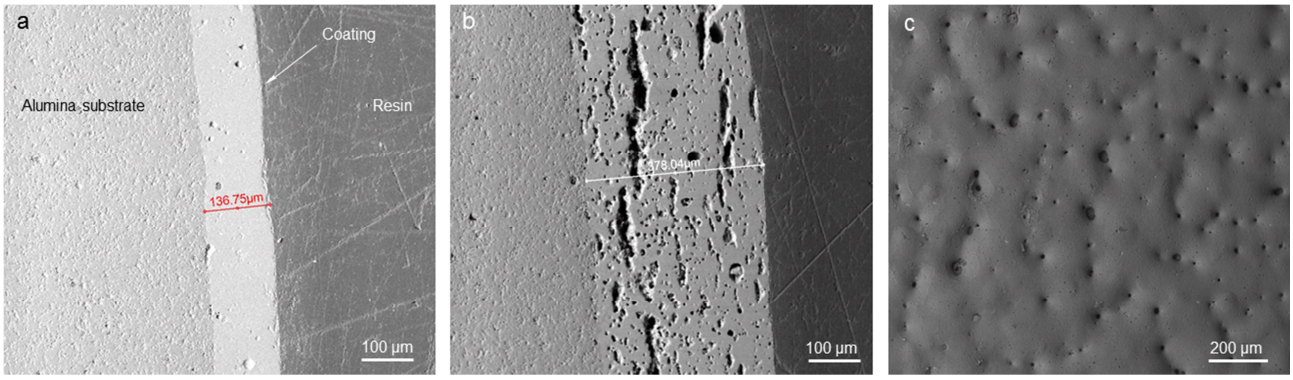

Fig. 3

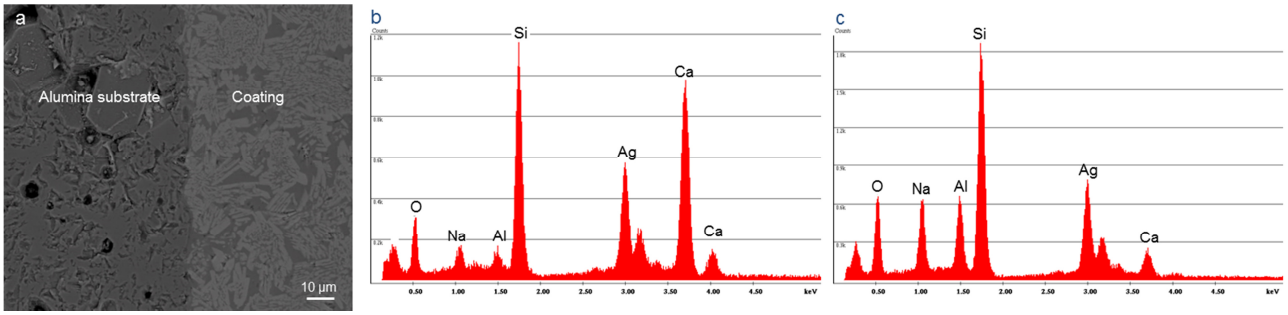

Fig. 4

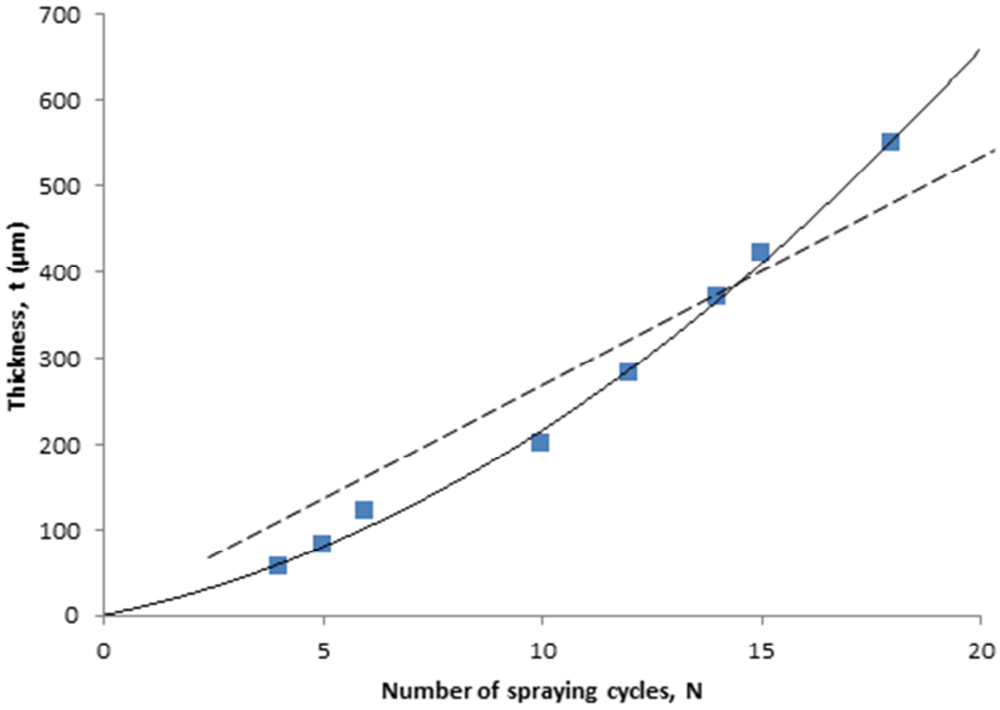

Fig. 5

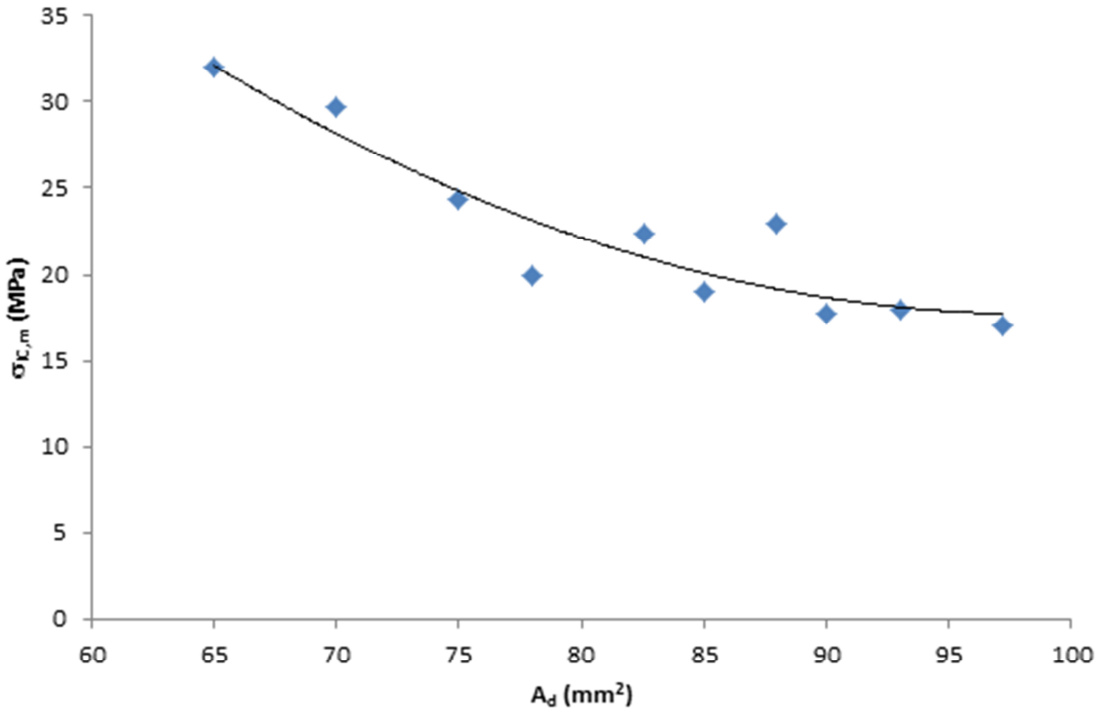

Fig. 6